Biol. Cybern. 88, 46–59 (2003)
DOI 10.1007/s00422-002-0330-5

Biological Cybernetics

An alternative approach to synthesizing bipedal walking

Herman van der Kooij[1], **Ron Jacobs**[2], **Bart Koopman**[1], **Frans van der Helm**[3]

[1]Institute of Biomedical Technology, University of Twente, PO Box 217, 7500 AE Enschede, The Netherlands
[2]Intelligent Inference Systems Corp., #107 West 333 Maude Avenue, Sunnyvale, CA 94086, USA
[3]Man–Machine Systems and Control Group, Delft University of Technology, Mekelweg 2, 2628 CD Delft, The Netherlands

Received: 25 May 2001 / Accepted in revised form: 8 April 2002

Abstract. Based on mechanical analysis, three gait descriptors are found which should be controlled to generate cyclic gait of a seven-link humanoid biped in the sagittal plane: (i) step length, (ii) step time, and (iii) the velocity of the center of mass (CoM) at push off. Two of these three gait descriptors can be chosen independently, since the CoM moves almost ballistically during the swing phase. These gait descriptors are formulated as end-point conditions and are regulated by a model predictive controller. In addition, continuous controls at the trunk and knees are implemented to maintain the trunk upright and to ensure weight bearing. The model predictive controller is realized by quadratic dynamic matrix control, which offers the possibility of including constraints that are exposed by the environment and the biped itself. Specifying step length and CoM velocity at push off, the controller generates a symmetric and stable gait. The proposed control scheme serves as a general-purpose solution for the generation of a bipedal gait. The proposed model contains fewer parameters than other models, and they are all directly related to determinants of bipedal gait: step length, trunk orientation, step time, walking velocity, and weight bearing. The proposed control objectives and the model of humanoid bipedal walking have potential applications in robotics and rehabilitation engineering.

1 Introduction

The synthesis of bipedal gait is a topic of interest in robotics as well as in biomechanics. During the past few decades several approaches have been published, and different 'bipedal walkers' have been constructed in attempts to predict or mimic human gait. Most 'predictive' models are complex, contain many parameters, demand tremendous computational effort, have poor stability properties, and do not give much additional insight in the control objectives needed to generate cyclic gait (e.g., Yamaguchi 1989; Van de Belt 1997; Pandy and Anderson 1999). In the field of robotics, most bipedal walkers require complex control schemes and consume much more energy than humans. Moreover, most bipedal walkers do not walk very 'naturally' (for an overview of bipedal walkers, see Sardain et al. 1998).

The different approaches used to synthesize bipedal gait can be roughly categorized as follows:

1. *Open-loop control*. This approach attempts to determine the control-input patterns (e.g., joint moments, muscle forces, or muscle activation) or joint trajectories that will result in a cyclic gait. Since information of the current system states is not fed back to the controller, the solutions are unstable. This approach is widely used in biomechanical computer simulations (e.g., Yamaguchi 1989; Koopman et al. 1995; Van de Belt 1997; Pandy and Anderson 1999). This approach is characterized by difficulties in finding feasible solutions and immense computation times (Yamaguchi 1990; Anderson et al. 1995).
2. *Trajectory control*. In this approach every joint trajectory during the cycle is prescribed. An important issue within this approach is trajectory planning. Sometimes these trajectories are derived from human walking (e.g., Yang 1997), from kinematic constraints (e.g., Lum et al. 1999), from coherent parameters characterizing human gait (Hurmuzlu 1993), or they are obtained using learning algorithms (e.g., Benbrahim and Franklin 1997; Salatian et al. 1997). It is important that the prescribed trajectories are feasible in that the biped does not fall forward or backward. To obtain such a trajectory the zero-moment-point control strategy (Vukobratovic and Stokic 1975) can be used. The local stability about the operation point (joint angle trajectories) is

Correspondence to: H. van der Kooij
(e-mail: h.vanderkooij@wb.utwente.nl, Fax: +31-53-4893471)

guaranteed utilizing feedback schemes. However, to ensure stability of walking, stability should not only be addressed with respect to prescribed trajectories. From our experience as humans, we all know that it is sometimes necessary to take smaller or larger steps when we are subjected to sudden perturbations, such as a push or stumble. In such situations a 'trajectory-tracking' strategy is not the best for preventing falling.

3. *Set-point control*. Rather than specifying all joint trajectories as a function of time, one can specify only the values at specific times. Biped locomotion has been realized by using linear state feedback and specifying the configuration of the biped at the end of the swing phase (Mita et al. 1984). The biped could only make small steps; for larger steps the difference between the biped's configurations at begin and end of the swing phase will be too large, and the linear feedback controller will be unstable. For the built biped, the motion of the center of mass (CoM) during the swing phase was (indirectly) controlled. However, when the CoM is relative high and the feet relative small, as in humans, the control of CoM motion is severely limited by the constraint that the feet should be flat on the ground (Kuo and Zajac 1993). By specifying set points in the support, the toe off, swing, and straighten phases cyclic gait can be generated off a seven-link, 12-degree-of-freedom biped (Pratt and Pratt 1999).
4. *Nonlinear dynamic system/ballistic walking approach*. In this approach, a cyclic gait pattern is the result of dynamical system properties (e.g., joint impedance and segment inertia) interacting with the environment. Ballistic walking down a slope is an old and well-known example of this system approach (e.g., McMahon 1984; McGeer 1990). The ballistic walking concept can be extended by including adjustable springs (van der Linde, 1999) or 'passivity-mimicking' control laws (Goswami et al. 1997). Taga (1995a, b) also demonstrated the capabilities of such a system approach. By entrainment of neural oscillators, the environment, and body mechanics, stable gait emerges. In the system approach, the system is structural stable for small disturbances. However, stability for larger disturbances is not guaranteed and not explicitly addressed.

In our opinion, existing models of bipedal walking and control schemes for bipedal walkers have one or more of the following problems:

1. The absence of a general-purpose solution for walking with various speeds and different stride length.
2. Complex model structures and/or control schemes. Most models contain a large number of parameters that are not directly related to determinants of bipedal gait. Most active control schemes use continuous controls to track fully specified trajectories. In our opinion this is not necessary; only those parameters that determine cyclic gait need to be controlled.
3. Poor cyclic stability properties. Different methods have been proposed for analyzing the stability of cyclic walking (Seo and Yoon 1995) and to enlarge the stability of bipedal walkers. However, compared with humans, existing models and robots have inferior stability properties. We think this is due to inflexible control laws and a lack of understanding of which parameters should be controlled.

This paper presents an alternative and relatively simple control scheme based on mechanical analysis of human gait. Controlling walking speed, step length, and weight bearing is sufficient for generating a stable cyclic gait in a seven-link humanoid biped in the sagittal plane. Walking speed and step length and/or time are regulated with an end-point controller. Weight bearing is regulated with continuous controls at the trunk and knees. Continuous and end-point controls are formulated within one control scheme. This approach can be best compared with Raibert's (1986) approach for hopping robots. He demonstrated very nicely that controlling hopping height, forward speed, and body attitude are sufficient for stable hopping and running of a walking machine. This paper differs from Raibert's approach in that the movement of the body parts between initial and end-point conditions are not specified. This allows the body parts to move relatively freely between the beginning and end of a phase, thereby exploiting their natural dynamics. The temporal aspects of the control objectives is also more explicitly addressed in this paper, and is a direct result of the ballistic characteristics of bipedal walking in the swing phase. However, the computations are far more demanding than Raibert's approach, although not too demanding to make this approach unsuited for real-time applications (see Sect. 4).

The joint angles, joint moments, and energy balance of the generated gait pattern are compared with those of a human subject. Humans are considered as living examples of how to walk. Comparing model predictions with human data provides an insight into differences and similarities between how the model and how humans walk. The comparison may result in improvements to control algorithms for synthesizing bipedal gait. The presented approach serves as a transparent theoretical framework in the understanding of bipedal gait.

Two important aspects of any control scheme that generates bipedal gait are its robustness and flexibility. To make a (future) comparison with other control schemes possible, task adaptation and robustness properties are evaluated. Robustness to structural changes of the biped itself is studied by simulating walking with a passive ankle, with a passive knee and ankle, and with constraints on the control torques. The flexibility of the proposed control scheme to changes in environmental constraints is examined by simulating uphill walking. The flexibility of the alternative control scheme for different step lengths and walking velocities is investigated by systematically varying the desired step length and velocity of the CoM at toe off.

2 Methods

2.1 Biped dynamics

A seven-link segment model is used to represent the biped's dynamics. The model is planar and accounts only for anterior–posterior motion of the body. The seven segments represent the trunk, the left and right thighs, the shank, and the foot (Fig. 1).

The mass, position of the CoM, moment of inertia, and length of each of the segments are scaled to the dimensions of a human (body mass 80 kg, length 1.90 m) using the regression equations of Chandler et al. (1975). The segments are connected by friction-free hinge joints, which are spanned with springs and dampers. The control inputs are torque actuators at each joint. The equations of motion are derived following Lagrangian formalism, and are given by

$$\mathbf{M}^q \ddot{\boldsymbol{q}} = \mathbf{f}^q \tag{1}$$

where $\mathbf{M}^q$ is the mass matrix, $\mathbf{f}^q$ is the vector of forces, and $\boldsymbol{q}$ is the vector of generalized coordinates. Passive structures – restricting the range of motion of a joint – are modeled as nonlinear springs and dampers. The characteristics of these springs and dampers are obtained from human data (Yoon and Mansour 1982; Mansour and Audu 1986).

Foot–floor interactions are modeled as soft constraints by springs and dampers at the ball and heel of the foot. The offset of the vertical spring depends on a given ground profile. When the toe or heel touches the ground, a dynamic friction force models the horizontal reaction force. When the contact point reaches zero velocity, the horizontal reaction force is modeled by a spring (see Appendix A). In this paper bipedal gait is divided into the double-support phase and the single-support or swing phase. In the model, the beginning of the double-support phase is defined as the moment at which the heel or toe of the previous swing leg reaches zero velocity. The end of the double-support phase is defined as the moment at which the toe of the back leg leaves the ground.

2.2 Synthesis of bipedal gait

To obtain a cyclic gait it is not necessary to control all joint angles as a function of time (Raibert 1986). Specifying end-point control objectives associated with both the forward speed of the CoM at the end of double-support phase, and the placement of the swing leg at the end of the swing phase, are sufficient to generate cyclic gait. In addition, continuous controls on the trunk and knees ensure an upright posture. In the proposed model, only those parameters that are all directly related to determinants of bipedal gait are controlled: step length, trunk orientation, step time, walking velocity, and weight bearing. This alternative control approach is the result of the mechanical analyses of gait:

1. Due to the large moment of inertia around the ankle, ankle moments can hardly accelerate or decelerate the CoM. When the weight-bearing knees remains straight and the trunk remains upright, the CoM will move ballistically during the swing phase.
2. When the CoM moves ballistically, the step length (S), the step time (T), and the speed of the CoM at push off (V_{TO}) have a unique relationship. For a specific configuration of the swing leg at heel contact (HC) and a specific V_{TO}, S can be reconstructed from specified T or vice versa (see Appendix B).
3. In the double-support phase V_{TO} has to be controlled to maintain a constant walking velocity. It is possible to derive the required V_{TO} from specified S and T.
4. When we would be able to control the gait descriptors (S, T and V_{TO}), it is intuitively felt that a cyclic gait will be generated. However, due to the ballistic nature of bipedal gait, from these three gait descriptors, only two descriptors can be chosen independently.

A control scheme for the synthesis of bipedal gait (Fig. 2) is proposed. From a higher center, two of the three gait descriptors are supplied to the global controller (GC). The GC reconstructs the dependent from the independent gait descriptors (Appendix B) and regulates the control objectives:

1. Step length (S) at the end of the swing phase with duration defined by the swing time (T). During swing the CoM is assumed to move ballistically around the

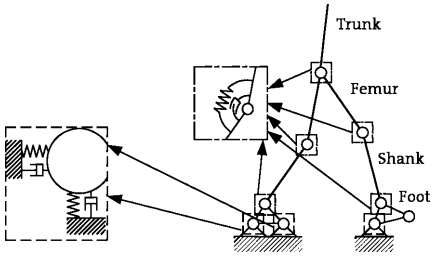

Fig. 1. Segment model

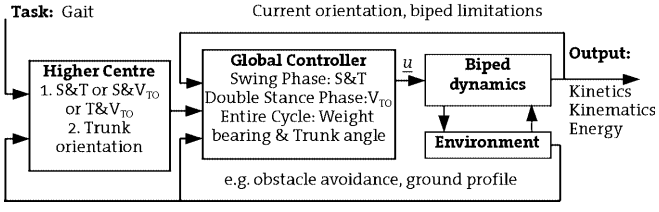

Fig. 2. Proposed model for the synthesis of bipedal gait. Two of the three gait descriptors are supplied from the higher center: the step length (***S***), the step time (***T***), and the velocity of the CoM at push off (V_{TO}). In addition the trunk orientation is supplied from the higher center to the global control. At the start of the swing or double-support phase the end conditions of the phase are reconstructed from these higher command signals. The global controller (GC) regulates end-point objectives in the swing phase (***S&T***) and double-stance phase (V_{TO}), and continuous objectives at the trunk and the knees (weight bearing). The calculated control inputs (joint moments) are applied to the model of the biped. The biped's current orientation and kinematics (maximal joint torques/joint powers) are fed back into the GC. Environmental conditions can expose constraints to the biped, which are supplied to the controller and the higher center

ankle. For a given velocity at push off (V_{TO}), the position of the CoM is known at the end of the swing time. Specifying the knee and ankle angle at foot contact, the thigh angle can be reconstructed, since at the end of the swing the feet have to be on the ground (Appendix B).
2. Horizontal velocity of the CoM at push off (V_{TO}). The duration of the double-support phase is specified.
3. Trunk orientation. In most conditions the trunk has to be maintained upright.
4. Weight bearing. To prevent collapsing, the knee joint of the leg that bears body weight has to be relatively straight during the entire cycle. The knee of the stance leg in the swing phase and the front knee in the double-support phase are controlled.

Control objectives 1 and 2 are end-point control objectives, and 3 and 4 are continuous control objectives. Therefore, a control algorithm is needed which can incorporate both types of control objectives. A model predictive control (MPC) is well suited to handling this mixture of control objectives.

2.3 Quadratic dynamic matrix control

The GC is implemented as an MPC, which uses an internal model of the system. Using a finite prediction horizon, future outputs of the system at discrete time steps are predicted as a function of last control inputs and future changes in control inputs. The MPC calculates the future changes in control inputs that minimize the differences between future and desired output. We implemented the MPC with quadratic dynamic matrix control (QDMC). This algorithm was developed by Garcia and Morshedi (1986) at the Shell Development Company for applications in the chemical industry. The algorithm utilizes a quadratic program (QP) to compute moves on process-manipulated variables in such a way that controlled variables are kept to their targets and violation of process constraints is prevented. QDMC is well suited to our control problem, since it is capable of handling a mixture of end-point and continuous control objectives. The mechanical system and the environment can expose constraints to the global controller, which can be incorporated using QDMC. With some modifications we adopted the QDMC algorithm described in Garcia and Morshedi (1986). Although QDMC is a linear controller, with some modifications it can be applied to nonlinear plants (Lee 1994). By successive linearization of the nonlinear mechanical system at the working point, future control inputs are found by solving a linear QP. The future control inputs are applied to the actual nonlinear mechanical system only for the next discrete time step. At the new working point, this procedure is repeated.

2.3.1 Formulation for single input–output systems. Since the final structures of the matrices used in QDMC are quite complex, for the sake of clarity the equations for a single-input, single-output system are formulated first. The derivation of Garcia and Morshedi (1986) is followed. Subtle changes make it necessary to present the QDMC equations used in our application. For a linear system, for any future discrete time $\bar{k}+m$, $m>0$, the output (y) is given by

$$y(\bar{k}+m)=\sum_{i=1}^{m} a_i \cdot \Delta u(\bar{k}+m-i)+y^*(\bar{k}+m) \tag{2}$$

where $\bar{k}$ denotes the present discrete time, Δu is the change in input variable or an input move, a_i is a unit step response coefficient of the system, and y^* is the output of the system in the case where the future control inputs equal past control inputs, i.e., the system's output for $\Delta u(\bar{k}+m-i)=0,\ i=1,\ldots,m$. The predictions of future outputs over a finite prediction horizon of P discrete time steps follows from (1), with $m=1,\ldots,P$:

$$\begin{bmatrix} y(\bar{k}+1) \\ \vdots \\ y(\bar{k}+P) \end{bmatrix} = \begin{bmatrix} y*(\bar{k}+1) \\ \vdots \\ y*(\bar{k}+P) \end{bmatrix} + \mathrm{A}\cdot \begin{bmatrix} \Delta u(\bar{k}) \\ \vdots \\ \Delta u(\bar{k}+P-1) \end{bmatrix} \tag{3a}$$

$$\mathrm{A}=\begin{bmatrix} a_1 & 0 & & 0 \\ a_2 & a_1 & & \\ \vdots & \vdots & \ddots & \\ a_P & a_{P-1} & \cdots & a_1 \end{bmatrix} \tag{3b}$$

where A is called the *dynamic matrix* of the system. The control problem is to find the changes in control inputs (Δu) that minimize the differences between future outputs and desired outputs (y_{ref}). Define a P-dimensional deviation vector $\boldsymbol{e}(\bar{k}+1)$ at time $\bar{k}+1$:

$$\begin{aligned} \boldsymbol{e}(\bar{k}+1) &= \boldsymbol{y}_{\mathrm{ref}}(\bar{k}+1)-\boldsymbol{y}^*(\bar{k}+1) \\ &= \begin{bmatrix} y_{\mathrm{ref}}(\bar{k}+1)-y^*(\bar{k}+1) \\ \vdots \\ y_{\mathrm{ref}}(\bar{k}+P)-y^*(\bar{k}+P) \end{bmatrix} \end{aligned} \tag{4}$$

and

$$\Delta \boldsymbol{u}(\bar{k})=[\Delta u(\bar{k})\cdots\Delta u(\bar{k}+P-1)]^{\mathrm{T}} \tag{5}$$

as a vector of P input moves.

The dynamic matrix control (DMC) problem is defined as finding the P future input moves $[\Delta \boldsymbol{u}(\bar{k})]$ so that the sum of squared deviations between predicted future outputs and the reference value ($\boldsymbol{y}_{\mathrm{ref}}$) is minimized. This is equivalent to the least-squares solution of

$$\boldsymbol{e}\big(\bar{k}+1\big)\equiv \mathrm{A}\cdot\Delta\boldsymbol{u}\big(\bar{k}\big) \tag{6}$$

By premultiplying (6) with A^{T}, the least-squares solution of (6) is

$$\Delta \boldsymbol{u}(\bar{k})=\big(\mathrm{A}^{\mathrm{T}}\mathrm{A}\big)^{-1}\mathrm{A}^{\mathrm{T}}e\big(\bar{k}+1\big) \tag{7}$$

2.3.2 Formulation for multivariable system. For a multiple-input, multiple-output system with n_u inputs and n_y outputs, (7) can still be applied. However, the matrices and vectors are redefined: A becomes a multivariable dynamic matrix composed of blocks of dimension $P \times P$ step response coefficients, as in (3b) relating the rth output to the sth input:

$$\mathrm{A} = \begin{bmatrix} A_{1,1} & A_{1,2} & \cdots & A_{1,nu} \\ A_{2,1} & A_{2,2} & \cdots & A_{2,nu} \\ \vdots & \vdots & & \vdots \\ A_{ny,1} & A_{ny,2} & \cdots & A_{ny,nu} \end{bmatrix} \tag{8}$$

The vector of variables of future input moves is redefined as

$$\Delta \boldsymbol{u}(\bar{k}) = [\Delta \boldsymbol{u}_1(\bar{k})^{\mathrm{T}} \Delta \boldsymbol{u}_2(\bar{k})^{\mathrm{T}} \cdots \Delta \boldsymbol{u}_{nu}(\bar{k})^{\mathrm{T}}]^{\mathrm{T}} \tag{9}$$

and $\boldsymbol{e}(\bar{k})$ becomes

$$\boldsymbol{e}(\bar{k}+1) = [\boldsymbol{e}_1(\bar{k}+1)^{\mathrm{T}} \boldsymbol{e}_2(\bar{k}+1)^{\mathrm{T}} \cdots \boldsymbol{e}_{ny}(\bar{k}+1)^{\mathrm{T}}]^{\mathrm{T}} \tag{10}$$

2.3.3 Weighting of input and output variables. The amplitude of input moves can be suppressed through the application of weighting factors for the input moves (Δu) and the demand that the sum of all weighted input moves is minimized. This can be incorporated in the DMC, so that (6) now becomes

$$\begin{bmatrix} \boldsymbol{e}(\bar{k}+1) \\ 0 \end{bmatrix} = \begin{bmatrix} \mathrm{A} \\ \boldsymbol{\Lambda} \end{bmatrix} \Delta \boldsymbol{u}(\bar{k}) \tag{11a}$$

where

$$\boldsymbol{\Lambda} = \mathrm{diag}(\overbrace{\lambda_1 \lambda_1 \cdots \lambda_1}^{|\longleftarrow \mathrm{P} \longrightarrow|} \lambda_2 \lambda_2 \cdots \lambda_2 \cdots \lambda_{nu} \lambda_{nu} \cdots \lambda_{nu}) \tag{11b}$$

and $\lambda_i > 0$ is the ith input-move suppression coefficient.

It is also possible to make a distinction between the importances of the different controlled output variables by weighting the least-squares residuals $[\boldsymbol{e}(\bar{k})]$. This is achieved by premultiplying the DMC equations (Eq. 6) with the matrix of output weights $\lambda_i > 0$:

$$\boldsymbol{\Gamma} = \mathrm{diag}\Big(\underbrace{\gamma_1 \gamma_1 \cdots \gamma_1}_{|\longleftarrow \mathrm{P} \longrightarrow|} \gamma_2 \gamma_2 \cdots \gamma_2 \cdots \gamma_{ny} \gamma_{ny} \cdots \gamma_{ny}\Big) \tag{12a}$$

End-point control can easily be incorporated in QDMC. An end-point objective is implemented by weighting these reference outputs with zeros for $k = 1, \ldots, P-1$, and with positive scalars for $k = P$:

$$\boldsymbol{\Gamma} = \mathrm{diag}\Big(\underbrace{0\ 0 \cdots \gamma_1}_{|\longleftarrow \mathrm{P} \longrightarrow|}\ 0\ 0\ \cdots \gamma_2 \cdots 0\ 0 \cdots \gamma_{ny}\Big) \tag{12b}$$

Including the weighting matrices on input moves and controlled output variables, the DMC equation becomes

$$\begin{bmatrix} \boldsymbol{\Gamma} \boldsymbol{e}(\bar{k}+1) \\ 0 \end{bmatrix} = \begin{bmatrix} \boldsymbol{\Gamma} \mathrm{A} \\ \boldsymbol{\Lambda} \end{bmatrix} \Delta \boldsymbol{u}(\bar{k}) \Leftrightarrow$$

$$\begin{bmatrix} \mathrm{A}^{\mathrm{T}} \boldsymbol{\Gamma}^{\mathrm{T}} \boldsymbol{\Gamma} \boldsymbol{e}(\bar{k}+1) \\ 0 \end{bmatrix} = \begin{bmatrix} \mathrm{A}^{\mathrm{T}} \boldsymbol{\Gamma}^{\mathrm{T}} \boldsymbol{\Gamma} \mathrm{A} \\ \boldsymbol{\Lambda}^{\mathrm{T}} \boldsymbol{\Lambda} \end{bmatrix} \Delta \boldsymbol{u}(\bar{k}) \Leftrightarrow$$

$$\mathrm{A}^{\mathrm{T}} \boldsymbol{\Gamma}^{\mathrm{T}} \boldsymbol{\Gamma} \boldsymbol{e}(\bar{k}+1) + 0 = \left(\mathrm{A}^{\mathrm{T}} \boldsymbol{\Gamma}^{\mathrm{T}} \boldsymbol{\Gamma} \mathrm{A} + \boldsymbol{\Lambda}^{\mathrm{T}} \boldsymbol{\Lambda}\right) \Delta \boldsymbol{u}(\bar{k}) \tag{13}$$

The least-squares solution of (13) is

$$\Delta \boldsymbol{u}(\bar{k}) = \left(\mathrm{A}^{\mathrm{T}} \boldsymbol{\Gamma}^{\mathrm{T}} \boldsymbol{\Gamma} \mathrm{A} + \boldsymbol{\Lambda}^{\mathrm{T}} \boldsymbol{\Lambda}\right)^{-1} \mathrm{A}^{\mathrm{T}} \boldsymbol{\Gamma}^{\mathrm{T}} \boldsymbol{\Gamma} \boldsymbol{e}(\bar{k}+1) \tag{14}$$

2.3.4 Handling of constraints. QDMC is a QP solution of the DMC equations. The advantage of a QP solution is that limits can be set on both the control input and controlled output variables. Constraints on control input variables are formulated as

$$\begin{bmatrix} -1_L & & \\ & \ddots & \\ & & -1_L \\ 1_L & & \\ & \ddots & \\ & & 1_L \end{bmatrix} \Delta \boldsymbol{u}(\bar{k}) \geq \begin{bmatrix} \left(\boldsymbol{u}_1(\bar{k}) - u_{1\max}\right) & \mathbf{1} \\ \vdots & \mathbf{1} \\ \left(\boldsymbol{u}_{ny}(\bar{k}) - u_{ny\max}\right) & \mathbf{1} \\ \left(\boldsymbol{u}_{1\min} - u_1(\bar{k})\right) & \mathbf{1} \\ \vdots & \mathbf{1} \\ \left(\boldsymbol{u}_{ny\min} - u_{ny}(\bar{k})\right) & \mathbf{1} \end{bmatrix}$$

with

$$1_L = \begin{bmatrix} 1 & 0 & 0 & \cdots & 0 \\ 1 & 1 & 0 & \cdots & 0 \\ \vdots & & & & \vdots \\ 1 & 1 & 1 & \cdots & 1 \end{bmatrix} \ (\mathrm{P} \times \mathrm{P}_{\mathrm{matrix}})$$

$$\mathbf{1} = (1\ 1\ \cdots\ 1)^{\mathrm{T}}\ (\mathrm{P} \times 1 \text{ column vector}) \tag{15}$$

where $u_{i\min}$ and $u_{i\max}$ are the lower and upper limits of the ith control input variable, respectively; and $u_i(\bar{k})$ is the present value of the ith control input variable. This inequality reflects that the sum of the current input move and all predicted future input moves should not exceed the maximum and minimum limits for all future time steps.

Constraints on controlled output variables are formulated as

$$\begin{bmatrix} -\mathrm{A} \\ \mathrm{A} \end{bmatrix} \Delta \boldsymbol{u}(\bar{k}) \geq \begin{bmatrix} \left(\boldsymbol{y}_{\mathrm{ref}}(\bar{k}+1) - \boldsymbol{y}_{\max}\right) \mathbf{1} - \boldsymbol{e}(\bar{k}+1) \\ \left(\boldsymbol{y}_{\min}(\bar{k}+1) - \boldsymbol{y}_{\mathrm{ref}}\right) \mathbf{1} + \boldsymbol{e}(\bar{k}+1) \end{bmatrix} = \begin{bmatrix} \boldsymbol{y} * (\bar{k}+1) - \boldsymbol{y}_{\max} \\ \boldsymbol{y}_{\min} - \boldsymbol{y}(\bar{k}+1) * \end{bmatrix} \tag{16}$$

where $\boldsymbol{y}_{\min}$ and $\boldsymbol{y}_{\max}$ are the lower and upper limits of the controlled output variables, respectively. This inequality reflects that future output variables should not exceed their maximum and minimum limits for all future time steps.

These constraints (Eqs. 15, 16) can be expressed as a system of linear inequalities:

$$C\Delta\boldsymbol{u}(\bar{k}+1) \geq \boldsymbol{c}(\bar{k}+1) \tag{17}$$

In addition, limits on individual input moves are defined as

$$\Delta\boldsymbol{u}_{\min} \leq \Delta\boldsymbol{u}(\bar{k}) \leq \Delta\boldsymbol{u}_{\max} \tag{18}$$

The least-squares solution of the DMC equations can be expressed as the quadratic minimization problem of equation

$$\min_{x(\bar{k})}\left(\frac{1}{2}\left[\mathrm{A}\Delta\boldsymbol{u}(\bar{k}) - \boldsymbol{e}(\bar{k}+1)\right]^{\mathrm{T}}\boldsymbol{\Gamma}^{\mathrm{T}}\boldsymbol{\Gamma}\left[\mathrm{A}\Delta\boldsymbol{u}(\bar{k}) - \underline{e}(\bar{k}+1)\right] + \frac{1}{2}\Delta\boldsymbol{u}(\bar{k})^{\mathrm{T}}\boldsymbol{\Lambda}^{\mathrm{T}}\boldsymbol{\Lambda}\Delta\boldsymbol{u}(\bar{k})\right) \tag{19}$$

In the absence of constraints the solution of (19) is given by (14). Including the inequality constraints (Eqs. 17, 18), the following QP has to be solved:

$$\min F = \frac{1}{2}\Delta\boldsymbol{u}(\bar{k})^{\mathrm{T}}\mathbf{H}\Delta\boldsymbol{u}(\bar{k}) - \boldsymbol{g}(\bar{k}+1)^{\mathrm{T}}\Delta\boldsymbol{u}(\bar{k})$$

subject to $C\Delta\boldsymbol{u}(\bar{k}) \geq \boldsymbol{c}(\bar{k}+1)$(constraint equation)

$\Delta\boldsymbol{u}_{\min} \leq \Delta\boldsymbol{u}(\bar{k}) \leq \Delta\boldsymbol{u}_{\max}$

in which (20)

$$\mathbf{H} = \mathrm{A}^{\mathrm{T}}\boldsymbol{\Gamma}^{\mathrm{T}}\boldsymbol{\Gamma}\mathrm{A} + \boldsymbol{\Lambda}^{\mathrm{T}}\boldsymbol{\Lambda}$$

and

$$\boldsymbol{g}(\bar{k}+1) = \mathrm{A}^{\mathrm{T}}\boldsymbol{\Gamma}^{\mathrm{T}}\boldsymbol{\Gamma}\boldsymbol{e}(\bar{k}+1) \tag{21}$$

2.4 Generation of gait

In order to generate a bipedal gait, the gait cycle was divided into the double-support and swing phases. At the beginning of these phases, the control objectives and duration of both the phases were reconstructed from higher-level commands (Fig. 2, Appendix B). These continuous and end-point control objectives define the output reference values ($\boldsymbol{y}_{\mathrm{ref}}$, Appendix C); the control inputs ($\boldsymbol{u}$) were the joint moments of force.

The control objectives were met by applying QDMC (Fig. 3):

0. From the desired duration of the phase and the sample time used by QDMC, the initial prediction horizon (P) is reconstructed.
1. After linearizing the mechanical system at the current state, a unit-step response model is obtained.
2. The weighting matrices are built from the control objectives and weights of control input and controlled output variables.
3. Integrating the nonlinear mechanical system with (as input) the last calculated control inputs gives a prediction of the system's output if the control input remains the same ($\boldsymbol{y}^*$). The deviation from the desired outputs can be calculated from $\boldsymbol{y}^*$ and desired output values ($\boldsymbol{y}_{\mathrm{ref}}$) if the control input remains the same [$\boldsymbol{e}(k+1)$].
4. The limits of the control inputs and combining the deviation vector[$\boldsymbol{e}(k+1)$] with the limits on the outputs result in a set of constraint inequalities.
5. All matrices and vectors are now known to solve the QP. The QP computes all moves on control input variables over the total prediction horizon (P). The future control inputs are reconstructed from the old control inputs.
6. From the future control inputs only the control inputs for the next discrete time step are selected. The actual (nonlinear) mechanical system is integrated with these control inputs (joint moments) to the next discrete time step.
7. The discrete time step is shifted from k to $k+1$, and the prediction horizon is shortened from P to $P-1$. The calculation sequence (steps 2–7) is then repeated.

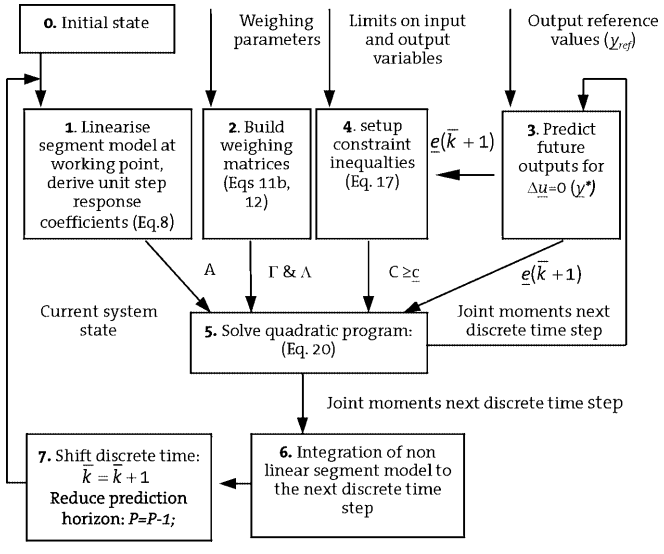

Fig. 3. Flow chart of the generation of bipedal gait; see text for explanation

3 Results

3.1 Generation of basic gait

Continuous controls at the trunk and knees, and end-point controls at the swing leg and at the horizontal velocity of the CoM at toe off generate a cyclic gait (Fig. 4). A linear spring and damper at the ankle joint stabilizes this joint (for simulation parameters, see Appendix C).

The desired CoM velocity at push off ($V_{\mathrm{TO}} = 1.25$ m/s) and the desired step length ($S = 0.75$ m) are supplied

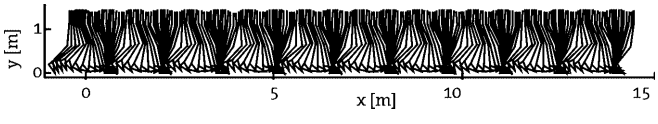

Fig. 4. Stick-figure walking movement, showing the first ten gait cycles. Only the right leg is displayed. The stick figure was traced every 0.05 s

to the GC from a higher center (Fig. 2). The specified double-support time was 0.17 s. From these gait descriptors a step time of $T = 0.42$ s is obtained. The resulting average walking speed is 1.28 m/s. From initial conditions (Figs. 4, 5), a symmetric cyclic gait is generated within one step (Fig. 5).

The resulting cyclic gait was not sensitive to small variations in initial conditions. Simulating one gait cycle required 40 s of CPU time on an HP900. Most of this was for the forward integration of the nonlinear mechanical system. Calculation of $\boldsymbol{y}^*$ took on average ~40%, and integration of the real system (Eq. 1) took ~45%.

Model-predicted joint angles are compared with measured joint angles of a human subject (body mass 80 kg, body length 1.9 m), walking at an average speed of 1.28 m/s (Fig. 6). Joint angles were averaged over the first ten cycles. Predictions of a 2-D model are compared with 3-D motion of a human subject who was not constrained to move in one plane. To make a comparison possible, the desired step length ($S = 0.75$) was chosen in such a way that the model-predicted hip angles at HC were approximately the same as those measured at HC. The subject's step length and step time were $S = 0.8$ m and $T = 0.57$ s. The predicted and measured joint angles of the hip and knee are similar. For humans, the ankle joint of the stance leg shows more plantar flexion in the earlier stance phase ($t \sim 0.14$–0.4 s).

In contrast with model predictions, at the end of the stance phase, humans lift their heel from the ground, thereby enlarging the step length (McMahon 1984). At the end of the double-support phase ($t \sim 0.58$–0.64 s), the model predicted plantar flexion of the ankle joint of the back leg is also smaller to that measured in humans. Foot clearance is not included in the controller as an environmental constraint, but knee flexion during the swing phase is sufficient.

For the subject, the joint moments of force are calculated using inverse dynamics (Koopman et al. 1995) and normalized to body weight. Human and model-predicted joint moments are compared in Fig. 7. Model-predicted and measured joint moments show similar features. In the double-stance phase and at the beginning of the swing phase ($t \sim 0.5$–0.7 s), hip flexion and knee extension moves the (future) swing leg forward. At the end of the swing phase ($t \sim 0.8$–1 s), hip extension and knee flexion torques decelerate the leg. Strong plantar flexion at the ankle joint moves the body forward during push off ($t \sim 0.5$–0.6). Although the model-predicted and measured patterns are quite similar, their timing is a little different. Real plantar flexion is much larger in the stance phase than predicted by the model. This can be explained by the previously found differences in ankle joint angles (Fig. 6). Whereas in the model the foot remains flat on the ground during single stance phase, in reality people roll their feet over ground. The amplitudes of model-predicted joint moments are larger than measured values. This can be explained by the fact that the impact losses for the planar model are larger than for a 3-D human. The difference between the foot rollover of the model and of humans can also be clearly seen in the ground reaction forces (Fig. 8). The foot rollover in the model shifts weight bearing from the left foot to the right foot less fluently than in humans, as can be seen from the high forces for the model at $t \sim 0$. Whereas in human walking the heel of the standing leg is already lifted from the ground in the middle of the stance phase ($t \sim 0.3$ s), causing a gradually increase of the vertical ground reaction force, the heel of the model foot remains flat on the ground and starts lifting from the ground at the beginning of the push-off phase

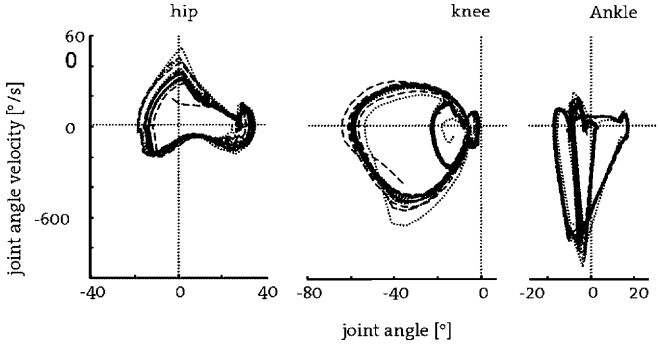

Fig. 5. Phase portraits of the hip, knee, and ankle joint angles for the first ten gait cycles. A steady state is reached within 1 cycle. The gait is symmetric: steady cycles of the right (*dashed lines*) and left legs (*dotted lines*) coincide

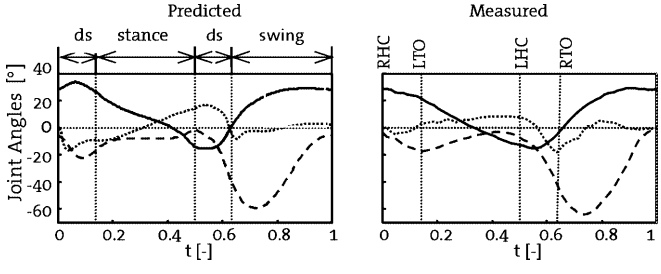

Fig. 6. Comparison of mean predicted and measured joint angles of the right hip (*solid lines*), knee (*dashed lines*), and ankle (*dotted lines*). Time is normalized to the cycle time. Hip and ankle flexions are positive, and knee flexion is negative. Right HC (*RHC*, at $t = 0$), left toe off (*LTO*, $t \sim 0.14$ s), left heel contact (*LHC*, $t \sim 0.5$ s) and right toe off (*RTO*, $t \sim 0.64$ s) are indicated in the graph by *vertical lines*, dividing a cycle into a double-support phase (*ds*), a stance phase, and a swing phase

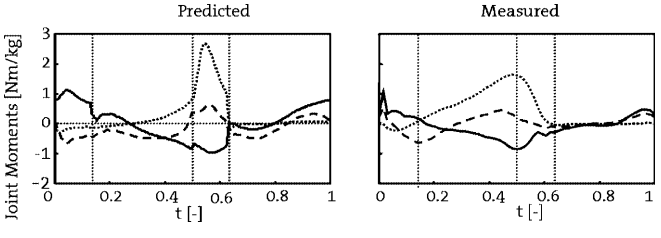

Fig. 7. Comparison of predicted and measured joint moments of the right hip (*solid lines*), knee (*dashed lines*), and ankle (*dotted lines*). Moments are normalized to body weight; time is normalized to the cycle time. Hip flexion is negative, and ankle plantar and knee flexions are positive

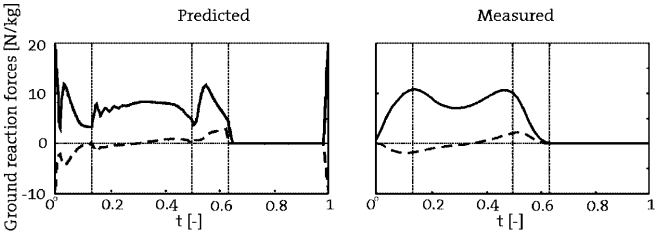

Fig. 8. Comparison of predicted and measured horizontal (*dashed lines*) and vertical (*solid lines*) ground reaction forces of the right leg. Forces are normalized to body weight; time is normalized to the cycle time

($t \sim 0.5$ s), after which the vertical ground reaction force of the model gradually increases.

Humans are known to walk very energy efficiently. To compare the energy consumptions of humans and the model, the joint powers of the model and a human subject (weight 80 kg, height 1.9 m) walking at the same velocity are compared. For the subject, the joint powers are calculated using inverse dynamics (Koopman et al. 1995). The integrals of positive and negative joint powers of a human subject for different phases of a gait cycle are shown in Table 1. The total positive energy for one gait cycle is 102.1 J. Normalized to body weight, the positive energy required per walking distance is Em = 0.80 J/kg·m. The largest amount of positive energy is needed to push off the body at the double-support phase (left leg push off: 30.2 J; right leg push off: 26.6 J). Although it is often assumed that the swing leg moves ballistically, considerable positive and negative energy is needed to move the swinging leg (Table 1: left swing, 9.0 J and −14.7 J; right swing, 6.6 J and −13.2 J.

The energy balance of a model-predicted bipedal gait (Table 2) is compared with the energy balance of a human subject (Table 1). For the model the positive energy required per walking distance, normalized to body weight, is Em = 1.79 J/kg·m, which is about two times larger than for a human subject (Em = 0.8 J/kg·m). The model needs more energy to push off than does a human subject (left leg push off: 70.9 vs 30.2 J; right leg push off: 69.8 J vs 26.6 J). The larger effort to push off can be explained by the large energy loss due to impact, indicated by the total difference between positive and negative energies for a whole cycle (51.9 J) and the much higher ground reaction forces of the model at impact compared to human walking data (Fig. 8). The larger impact loss in the model is also seen in the total absorbed energy in the front leg in the double-support phase (left push off: −8.4 J vs −25.6 J; right push off 7.0 J vs −26.7 J). Extension of the model to 3-D and

Table 1. Time integrals of positive and negative joint powers (in joules) of a human subject, based on measurements, walking at a velocity of 1.28 m/s. For the human subject, the joint powers are calculated using inverse dynamics. Sums of joint powers are given for the different phases in a gait cycle and for a whole gait cycle. Joint powers are given for each individual joint, for the right and left legs, and for both legs

Phase		Rhip (J)	Rknee (J)	Rankle (J)	Rleg (J)	Lhip (J)	Lknee (J)	Lankle (J)	Lleg (J)	Rleg + Lleg (J)
L. Push off	positive	2.3	1.4	0.6	4.2	5.7	1.1	23.49	30.2	34.5
	negative	−0.3	−5.0	−3.1	−8.4	−0.1	−3.4	0	−3.5	−11.9
L. Swing	positive	1.7	4.6	2.0	8.3	7.1	1.2	0.7	9.0	17.3
	negative	−7.4	−2.3	−7.6	−17.2	−1.6	−12.5	−0.6	−14.7	−32.0
R. Push off	positive	6.0	1.9	18.7	26.6	2.8	3.4	1.7	7.9	34.5
	negative	−0.2	−3.2	0	−3.5	−0.4	−5.2	−1.4	−7.0	−10.5
R. Swing	positive	5.6	0.3	0.7	6.6	1.7	7.1	0.5	9.3	16.0
	negative	−0.3	−12.2	−0.6	−13.2	−5.2	−0.7	−18.7	−24.6	−37.8
			Cycle positive:		45.7				56.4	102.1
			Cycle negative:		−42.3				−49.8	−92.1
			Cycle total		3.5				6.6	10.1

Table 2. Time integrals of positive and negative joint powers (J) of the model walking at a velocity of 1.28 m/s. Sums of joint powers are given for the different phases in a gait cycle and for a whole gait cycle. Joint powers for each individual joint, for the right and left legs, and for both the legs are given

Phase		Rhip (J)	Rknee (J)	Rank (J)	Rleg (J)	Lhip (J)	Lknee (J)	Lank (J)	Lleg (J)	Rleg + Lleg (J)
L. Push off	Positive	7.4	2.6	1.4	11.5	17.2	16.8	36.9	70.9	82.4
	Negative	−7.8	−11.6	−6.2	−25.6	−2.2	−1.4	−6.4	−10.0	−35.6
L. Swing	Positive	5.2	6.6	0.6	12.4	3.4	7.4	0.3	11.1	23.5
	Negative	−16.5	−0.4	−4.8	−21.7	−0.8	−21.1	−3.7	−25.6	−47.3
R. Push off	Positive	17.4	16.0	36.4	69.8	7.8	2.5	1.4	11.7	81.5
	Negative	−2.7	−0.6	−6.4	−9.7	−8.3	−12.2	−6.2	−26.7	−36.4
R. Swing	Positive	4.9	7.8	1.2	14.0	6.8	7.3	0.6	14.6	28.6
	Negative	−0.6	−22.3	−3.0	−26.0	−14.6	0.0	−4.3	−18.9	−44.9
			Cycle positive:		107.6				108.3	216.0
			Cycle negative:		−82.9				−81.2	−164.0
			Cycle total:		24.7				27.2	51.9

smoother transition between the swing phase and double-support phase is expected to reduce the impact loss and thereby the total required positive energy during push off. A smoother transition at HC can be achieved by realization of a foot rollover during swing phase that is more human-like.

The energy absorbed by the knee of the swing leg is much larger in the model than for a human subject (left swing: J −21.1 vs −12.5 J; right swing: −22.3 J vs −12.2 J). The difference is mainly caused by the passive spring and damper around the knee in the model ($K = 35$ Nm; $D = 3$ Nm/s).

3.2 Robustness to structural changes in the skeletal system

Humans are able to walk under a wide variety of challenging conditions. The capability of prosthetic walkers to adapt to their new situation demonstrates the extreme flexibility of the human nervous system. This adaptation demands intensive rehabilitation, especially for above-knee amputees. To investigate whether the model is able to walk in similar challenging conditions, below- and above-knee amputation is simulated by removing the active controls around the ankle and knee. Walking with limited muscle torques (cf. reduced muscle strength in humans) is simulated by constraining the active joint moments.

3.2.1 Walking with constrained joint torques. Active controls at all joints are constrained to -60 Nm $< \boldsymbol{u} < 60$ Nm. The specified step length is $S = 0.75$ m, and the specified velocity at toe off is $V_{TO} = 1.25$ m/s. When the active controls are not constrained, maximal active control torques at the hip, knee, and ankle are 92, 17, and 140 Nm for these objectives. Minimum active controls at the hip, knee, and ankle are −118, −66, and −7 Nm when the active controls are not constrained. When the active control is constrained, the average CoM velocity at toe off is $V_{TO} = 1.18$ m/s, the average walking velocity is $v = 1.14$ m/s, and the average step length is $S = 0.7$ m. Due to limited active control torques, the specified control objectives for V_{TO} and S are not met. Surprisingly, cyclic gait is still generated.

Compared to walking with unconstrained control inputs, the hip and ankle joint moments for walking with constrained control inputs are smaller (Fig. 9). However, the knee moments in the single-stance phase ($t \sim 0.15$–0.5 s) are larger for walking with constrained control inputs. Note that the absolute joint moments are larger than 60 Nm. Since the joint moments are the sum of active control torques and passive torques (springs and dampers), the resulting joint moments can be larger than 60 Nm or smaller than −60 Nm.

3.2.2 Walking with a passive left ankle. In this case active controls around the left ankle are removed, and the passive left ankle consists of a linear spring and damper ($K = 173$ Nm/rad; $D = 0.88$ Nms/rad). Again,

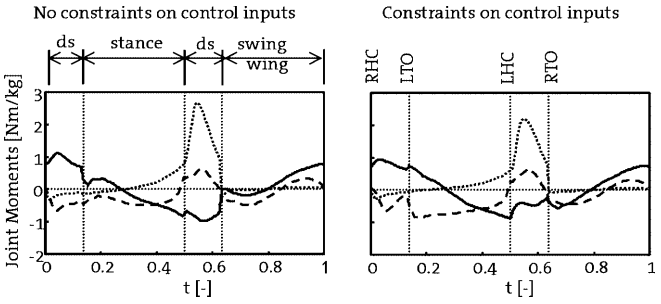

Fig. 9. Comparison of joint moments when the amplitude of the control inputs are constrained to -60 Nm $< \boldsymbol{u} < 60$ Nm (*right panel*) and when the control inputs are not constrained (*left panel*), for the right hip (*solid lines*), knee (*dashed lines*), and ankle (*dotted lines*). Moments are normalized to body weight; time is normalized to cycle time. Hip flexion is negative, and ankle plantar and knee flexions are positive

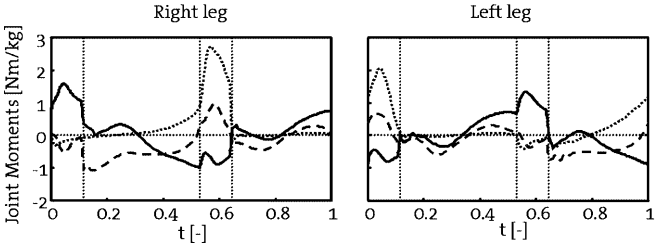

Fig. 10. Simulation of walking with a passive left ankle, showing joint moments of the right and left hips (*solid lines*), knee (*dashed lines*), and ankle (*dotted lines*). Moments are normalized to body weight; time is normalized to cycle time. Hip flexion is negative, and ankle plantar and knee flexions are positive

the desired CoM velocity at push off ($V_{TO} = 1.25$ m/s) and the desired step length ($S = 0.75$ m) are supplied to the model. For these reference values, the resulting average walking velocity is $v = 1.13$ m/s, and the average step length is $S = 0.78$ m. Step lengths are similar for the right and left legs, but step times (T) are asymmetric ($T = 0.50$ and 0.55 s, respectively). Push off with the left leg is affected by loss of active control around the left ankle: the velocity at push off (V_{TO}) is lower than specified. Consequently, to obtain the same step length the swing time of the left leg is larger. Note that in this paper, S and V_{TO} are supplied as reference values; if for example T and V_{TO} are supplied, a symmetric step time and an asymmetric step length are expected.

The absence of active controls at the left ankle can clearly be seen in the predicted joint moments (Fig. 10). The ankle moments of the right ankle are larger than of the passive left ankle, and the hip moments are larger than in normal walking.

3.2.3 Walking with a passive left ankle and a passive knee. In this case active controls around the left ankle and knee are removed. The stiffness and damping of the passive ankle joint are the same as in Sect. 3.2.2. The passive left knee is locked during the left stance phase and unlocked during the other phases. Knee locking is realized by a stiff spring and large damper around the artificial knee ($K = 333$ Nm/rad; $D = 9$ Nms/rad). When

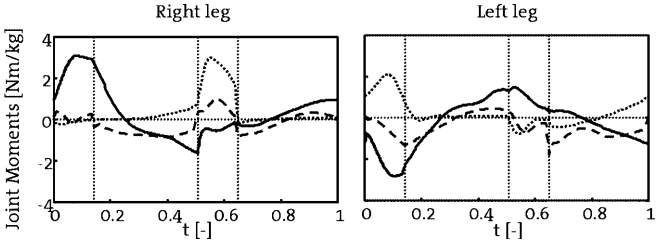

Fig. 11. Simulation of walking with a passive left knee and ankle, showing the joint moments of the right and left hips (*solid lines*), knee (*dashed lines*), and ankle (*dotted lines*). Moments are normalized to body weight; time is normalized to cycle time. Hip flexion is negative, and ankle plantar and knee flexions are positive

the knee is unlocked the stiffness around the ankle is $K = 55$ Nm/rad, and the damping is $D = 7$ Nms/rad. For an average walking speed of $V = 1.03$ m/s the step length for the right leg is $S = 0.56$ m and that for the left leg is $S = 0.67$ m. The step times are similar for the right and left legs ($T = 0.38$ s). Apparently, the model has some difficulties in regulating step length. In order to obtain a cyclic gait, the desired velocities at push off (V_{TO}) are chosen differently for the left and right legs: for the right leg $V_{TO} = 1.1$ m/s, and for the left leg $V_{TO} = 1$ m/s. The model becomes unstable when the same V_{TO} is supplied for the left and right legs, since the desired V_{TO} for left toe off cannot be obtained due to loss of active controls at the left leg.

The ankle moments of the left leg are much smaller than for the right leg in the double-support phase (Fig. 11). Whereas the right knee produces a flexion torque during push off, the left knee produces an extension torque. The hip moments are much larger than for the results of normal walking (Fig. 7, left panel).

3.3 Flexibility to changes in tasks and environmental constraints

The effects of changes in tasks and in environmental constraints on the proposed control scheme for generating walking was investigated. Walking uphill is an example of a change in environmental constraints; walking with various walking speeds and step lengths are examples of changing tasks.

3.3.1 Walking uphill. For walking over level ground the swing leg is specified to be straight at the end of the swing phase. However, for walking uphill this is not desired. Instead, specifying the shank to be vertical at the end of the swing phase will give a more appropriate configuration of the swing leg at the end of swing.

With this modification the model walks up a slope of $r = 0.1$ with an average progression speed of $V = 1.05$ m/s and a step length of $S = 0.51$ m (Fig. 12). (Note that r is the direction coefficient of the slope, with a value $r = 0.1$ corresponding to a slope of 5.7°, i.e., atan(0.1/1).) As expected, the required positive energy (Em = 5.27 J/m·kg) per unit distance is much larger than for level walking (Em = 1.79 J/m·kg). Em is defined as the time integral of the positive joint powers over a complete

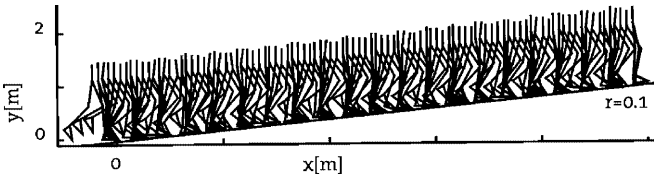

Fig. 12. Walking up a slope of $r = 0.1$. The stick diagram was traced every 0.1 s. Average walking speed was 1.05 m/s, step length was 0.51 m, and the sum of positive joint powers per walking distance is Em = 5.27 J/m·kg

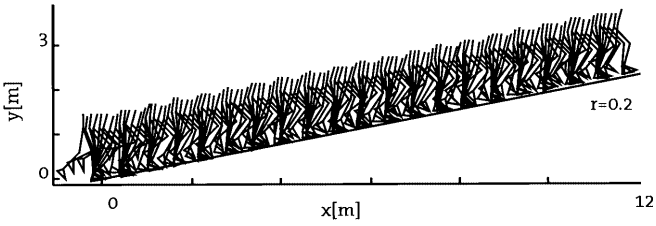

Fig. 13. Walking up a slope of $r = 0.2$. The stick diagram was traced every 0.1 s. Average walking speed was 1.05 m/s, step length was 0.62 m, the sum of positive joint powers per walking distance is Em = 6.5 J/m·kg

gait cycle, divided by the stride length and body weight. For larger slopes the model falls backwards; the knee flexion at HC increases when the step length remains constant. Consequently, larger knee moments are needed to extend the knee. To prevent falling for larger slopes, the distance between the horizontal position of the CoM and the foot in the swing phase should be reduced. This can be realized by bending the trunk forward. By specifying a trunk orientation of 10° instead of 0°, the model is able to walk up a slope of $r = 0.2$ with an average progression speed of $V = 1.05$ m/s and a step length of $S = 0.62$ (Fig. 13). The required positive energy per unit distance is Em = 6.5 J/m·kg. When the trunk is specified to be upright, the model falls backward. An alternative to forward trunk bending is reducing the step length. As a consequence of the larger energy required for walking uphill, the moments during the double-support phase increase. To prevent the model from 'flying,' the desired velocity at toe off (V_{TO}) has to be reduced for larger slopes. An alternative is to increase the double-support time.

3.3.2 Walking with various stride lengths at various velocities. Humans can walk at different combinations of walking speeds and step lengths. Combinations of feasible walking velocities and step lengths of the model are determined by systematically varying these descriptors. The flexibility of the model to adjust its step length is demonstrated by its ability to walk asymmetrically (Fig. 14).

Step length (S) and horizontal CoM velocity at toe off (V_{TO}) are supplied as reference values. S is systematically changed from 0.5 m to 0.85 m with small increments. This is also done for $V_{TO} = 0.8, 0.9, \ldots, 1.5$ m/s. Recall that T can be reconstructed from S and V_{TO}. The model walks for a wide range of different step lengths and

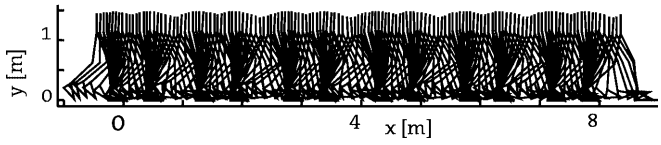

Fig. 14. Stick diagram for asymmetric walking, with the stick traced every 0.005 s. Left leg took large steps ($S = 0.89$, $T = 0.42$), and right leg took small steps ($S = 0.58$, $T = 0.46$); $v = 1.23$ m/s

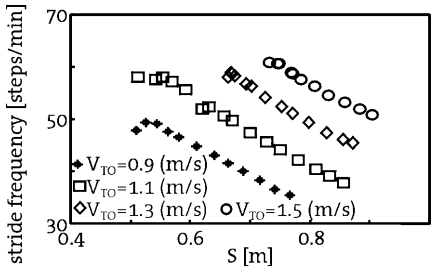

Fig. 15. Relation between step length (S) and stride frequency at different velocities at push off (V_{TO})

walking velocities (Fig. 15). The almost linear relation between step length and stride frequency at a specific walking velocity (Fig. 15) is also seen in human walking (Grieve and Gear 1966). This figure also shows that for faster walking the minimal feasible step length increases. For large walking velocities and small step lengths, the swing leg has to move forward very fast (i.e., small T), which causes problems for very fast movements. For small walking velocities, the maximal feasible step length decreases (Fig. 15). When a step is too large and the velocity is too low, the body falls backward like an inverted pendulum with an initial velocity that is too low.

Although humans are able to walk at various combinations of progression speed and step length, they tend to walk with a specific step length at a specific speed (Inman et al. 1981). For a specific CoM velocity at push off, the positive energy cost per unit distance (Em) depends on the step length (Fig. 16), and there is an optimal step length (S^*) for which Em shows a minimum (Em^*). The optimal step length scales linearly with walking velocity (Fig. 17). The relation found in humans between step length and walking velocity is also linear (Koopman 1989). The required positive energy per walking distance (Em^*) when walking with the optimal step length (S^*) increases for larger walking velocities (Fig. 18). This is in agreement with experimental data of a human subject (Fig. 18).

4 Discussion

We have presented a general-purpose solution for generating bipedal gait. A cyclic gait was generated by regulating only a few descriptors of the gait. The predicted joint angles and moments resemble those of humans. The total positive energy required for the model to walk is about 2 times larger than in a human subject walking with the same velocity. In this paper

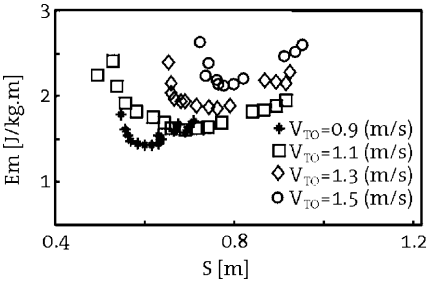

Fig. 16. Model-predicted sums of positive joint powers per walking distance (Em) for different CoM velocities at push off (V_{TO}) and step lengths (S). Sums of joint powers are normalized to body weight

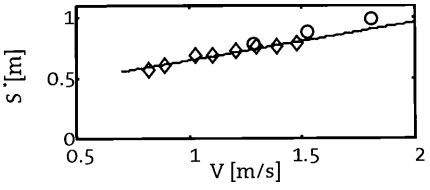

Fig. 17. Model-predicted optimal step length S^* at different walking speeds, V (*diamonds*). The relation between S and V is approximated by a least-squares fit of $S^* = aV + b$ (*solid line*; $a = 0.31$; $b = 0.33$). The step lengths of a human subject (weight 80 kg, height 1.90 m) at three different walking speeds are also shown (*circles*, experimental data)

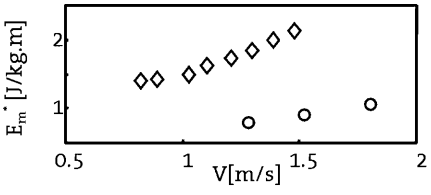

Fig. 18. Model-predicted sum of positive joint powers per walking distance (Em^*) at optimal step length S* at different walking speeds V (*diamonds*). The sums of positive joint powers of a human subject (weight 80 kg, height 1.90 m) at three different walking speeds are also shown (*circles*, experimental data). Sums of joint powers are normalized to body weight

the focus was on the control objectives that are needed to generate cyclic gait and not on the energy consumption of gait. Energy consumption was not included in the object function of the MPC. The gait descriptors that are controlled have a clear correspondence to the determinants of cyclic gait: step length, progression speed, stride time, weight bearing, and orientation of the upper body. This paper also shows that there is no need to control all joint angles as a function of time.

The number of model parameters is smaller than in other models, and the control objectives are clear and transparent. Other models (Yamaguchi 1989; Van de Belt 1997; Pandy and Anderson 1999) try to find a sequence of input patterns (e.g., joint moments, muscle forces, or muscle activations) that generates cyclic gait with minimal energy consumption. Hundreds of variables are found by optimization. The solutions are unstable since no feedback is incorporated, and hence the solutions do not give

insight in the control objectives underlying bipedal walking; the intelligence is in the optimization algorithms. The models developed by Taga (1995a) include (non-conventional) feedback. However, the numerous feedback gains are difficult to relate to the gait pattern. In all aforementioned models it takes much effort – trial and error and immense computation times – to find feasible solutions (e.g., Anderson et al. 1995; Yamaguchi 1990). In the present approach it is clear which variables are controlled, in contrast with other computer models. By controlling these parameters cyclic gait is guaranteed, without significant trial and error and with modest computation times compared to the aforementioned models.

4.1 Towards efficient walking

In ballistic walking cyclic gait is the result of an interaction between a neuromechanical system and the environment. Energy losses mean that energy has to be supplied to the system. In earlier concepts of ballistic walking this energy was supplied by gravity, limiting the approach to walking downhill. By triggered (van der Linde 1999) or constant input forces (McGeer 1990), 'ballistic walking' on level ground can be generated. Adjusting the control inputs can generate various types of gait with different speeds and step lengths. In most ballistic walkers, feedback is not incorporated. This makes it difficult to find a cyclic gait and it limits the region of stability, especially when the number of degrees of freedom increases.

The basic idea of ballistic walking is to walk with minimal energy consumption by using optimally the mechanical properties of the biped and the mechanical interactions of the biped with the environment. This basic idea can be incorporated into the presented model. The intriguing question is then whether the control effort of the GC (active joint moments) can be minimized by adjusting the passive properties of the mechanical system. The dynamics of the mechanical system could be adjusted such that for a given step length and walking speed, energy is optimally stored and freed in elastic elements, and energy is optimal transferred across joints by biarticular springs (Van Ingen Schenau 1989). This concept can be extended with triggered or reflex-like input or muscle actions, acting as a low-level or peripheral controller (van der Linde 1999). Ideally, the GC is supervising the generation of gait, whereas the actual gait is generated by the interaction of the mechanical system and the environment and controlled by low-level triggered control actions. The global control ensures stability, especially in the case of perturbations or sudden changes in task and environmental constraints.

4.2 Real-time applications

In our approach it is not necessary to prescribe all individual joint trajectories, in contrast with most control schemes of existing bipedal walkers. Prescribing consistent end-point conditions for the CoM velocity at push off and the swing leg at HC, as well as continuous controls on the knees and trunk, are sufficient to generate bipedal gait. However, the required computation time is too large for real-time control of a biped. Most of the CPU time is used for integrating the nonlinear equations to calculate the system's output (Y^*) for $\Delta U = 0$. The use of lookup tables or parallel computing will drastically reduce the processing time. Moreover, the use of QDMC is not the backbone of our concept; the main message is that controlling progression speed and step length at push off and HC, respectively, in combination with continuous control at the trunk, is sufficient to generate cyclic gait. Other control schemes might be well suited to meeting the same control objectives. Reduction of CPU time and real-time applications will be a topic of future research.

4.3 Flexibility and robustness of the proposed control scheme

The proposed control scheme was robust to structural changes in the skeletal system. Cyclic gait with one passive ankle and/or knee is generated without adjusting the structure of the control scheme. To be of use in the design process of new and prosthetic systems, the model should be able to generate a cyclic gait without active controls at the ankle and/or knee. The preliminary results presented in this paper are promising. Further research has to explore the possibilities and benefits of the proposed control scheme in the design process. Whether the assumptions underlying the proposed control scheme are valid for normal and pathological human walking is still an open question.

Controlling the walking velocity is possible by varying the desired velocity of the CoM at the end of double support. Controlling the step length is possible by varying the desired step length. Variation of only two end-point objectives generates various types of gait. For the proposed control scheme there is no need to adjust the planning of desired trajectories when desired speed or step length is altered, in contrast with conventional control schemes were trajectory planning and control are separated. Except for the trunk orientation and knee angle, the joint trajectories are not defined between the beginning and the end of the double-support or swing phase. Most joints are relatively 'free' during these phases. By varying only two variables directly related with speed and step length, the proposed control scheme is very flexible.

Although various combinations of walking speeds and step lengths are possible, the energetic costs differ. For a specific speed, the required energy per unit distance depends on the step length. For every speed there is an optimal step length which requires less energy per unit distance than other step lengths. For larger walking velocities the optimal step length increases. This relation between step length and walking speed is also seen in human walking (Koopman 1989). The minimal energy per unit distance – energy for the optimal step length – depends on the walking velocity.

5 Conclusion

We have developed a general-purpose solution for the generation of biped gait. Only a few control objectives are regulated by an MPC: (i) trunk orientation, (ii) knee angle of the leg that bears body weight, (iii) horizontal velocity of the CoM at the end of the double-support phase, and (iv) the configuration of the swing leg at the end of the swing phase. Objectives iii and iv are reconstructed from the gait descriptors: step length, step time, and walking velocity. Since the CoM moves ballistically during the swing phase, two of these gait descriptors can be chosen independently. Environmental and bipedal constraints can easily be incorporated into the MPC.

Task adaptation and robustness to changes in skeletal dynamics were evaluated. Using only four control objectives, this control scheme was able to generate a cyclic gait at various combinations of speeds, step lengths, and step frequencies. The model was even able to walk uphill, asymmetrically, and with passive knees and ankles.

Appendix A: Foot–floor interactions

The horizontal and vertical reaction forces at the heel and toe are given by

$$F_{\mathrm{gy}}^{\mathrm{heel,toe}} = \left\{K_{\mathrm{gy}}[y^{\mathrm{heel,toe}} - f_{\mathrm{gy}}(x^{\mathrm{heel,toe}})] + D_{\mathrm{gy}}\dot{y}^{\mathrm{heel,toe}}\right\} \, l[y^{\mathrm{heel,toe}} - f_{\mathrm{gy}}(x^{\mathrm{heel,toe}})] \quad \text{(A1)}$$

$$\text{if} \quad \left|F_{\mathrm{gx}}^{\mathrm{heel,toe}}\right| \leq \left|\mu F_{\mathrm{gy}}^{\mathrm{heel,toe}}\right| \Rightarrow$$
$$F_{\mathrm{gx}}^{\mathrm{heel,toe}} = \left[K_{\mathrm{gx}}(x^{\mathrm{heel,toe}} - f_{\mathrm{gx}}) + D_{\mathrm{gx}}\dot{x}^{\mathrm{heel,toe}}\right] \, l[y^{\mathrm{heel,toe}} - f_{\mathrm{gy}}(x^{\mathrm{heel,toe}})] \quad \text{(A2)}$$

$$if \ \dot{x}^{\mathrm{heel,toe}} \neq 0 \Rightarrow F_{\mathrm{gx}}^{\mathrm{heel,toe}} = \mu F_{\mathrm{gy}}^{\mathrm{heel,toe}} m(\dot{x}^{\mathrm{heel,toe}}) \quad \text{(A3)}$$

$$l(x) = 0 \ for \ x \geq 0; \ \ l(x) = 1 \ for \ x < 0 \quad \text{(A4)}$$

$$m(x) = -1 \ for \ \dot{x}^{\mathrm{heel,toe}} > 0; \ \ m(x) = 1 \ for \ \dot{x}^{\mathrm{heel,toe}} < 0 \quad \text{(A5)}$$

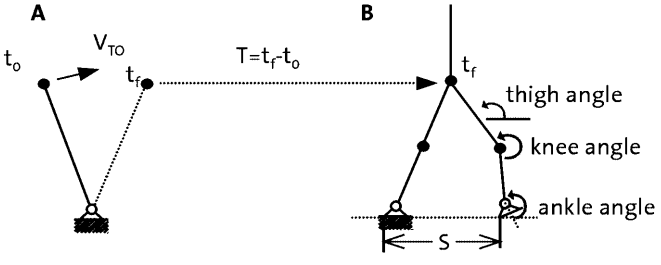

Fig. 19. A During the stance phase the CoM moves ballistically. The initial position and velocity, and the CoM position at the end of the swing phase are known. B Hip position is reconstructed from CoM position. Since at the end of the swing phase the heel should make floor contact, the thigh angle can be reconstructed from the known hip position and the specified ankle and knee angle

where $x^{\mathrm{heel,toe}}$ and $y^{\mathrm{heel,toe}}$ are the positions of the heel and toe. K_{g} and D_{g} represent the stiffness and damping, f_{gy} is a ground profile function, f_{gx} is the offset of the horizontal springs, and μ is the friction coefficient. When the heel or toe touches the ground, the horizontal reaction force is modeled as a dynamic friction force (Eq. A3). When the toe or heel reaches zero horizontal velocity, the horizontal reaction force is modeled by a spring and damper (Eq. A2). The offset of this spring (f_{gx}) is the position of the heel or foot at which it reached zero horizontal velocity. However, when this horizontal reaction force is larger than the maximal friction force, the horizontal reaction forces are modeled as dynamic friction forces (Eq. A3).

Appendix B: Relation between S, T, and V_{TO}

The CoM is assumed to move passively during the swing phase, since due to the large moment of inertia around the stance leg's ankle, ankle moments hardly influence CoM motion during this phase. CoM motion during the swing phase is modeled as an inverted pendulum. The body mass is concentrated at the end of the pendulum, and the rod has no mass. When the CoM position and velocity (V_{TO}) at the begin of the swing phase (t_0) is known, the position of the CoM at the end of the swing phase (t_f) can easily be calculated (Fig. 19A).

The hip position is known from CoM position. By specifying knee and ankle angles of the swing leg at the end of swing phase, the thigh angle can be reconstructed and the step length (S) is calculated (Fig. 19B), since by definition the HCs ground at the end of swing.

So, for a given V_{TO} and T, S can be reconstructed. Reconstruction of V_{TO} from S and T, or T from S and V_{TO} is straightforward.

Appendix C: Simulation parameters

The parameters for foot–floor interaction (Eqs. A1–A5) were as follows: the stiffnesses of horizontal and vertical springs were $K_{\mathrm{gx}} = 1 \times 10^5$ and $K_{\mathrm{gy}} = 1 \times 10^6$, and the damping factors were $D_{\mathrm{gx}} = 1 \times 10^3$ and $D_{\mathrm{gy}} = 1 \times 10^4$, respectively. The friction coefficient was $\mu = 0.5$. The stiffness and damping of the various joints are given in Table C1.

For the shown gait patterns, the specified double-stance time was 0.17 s. The duration of the swing phase

Table C1. Parameters of springs and dampers acting across different joints

Joint	K (Nm)	D (Nm/s)	Joint	K (Nm)	D (Nm/s)
Swing Hip	5	4	Front Hip	5	4
Stance Hip	5	4	Back Hip	5	4
Swing Knee	35	3	Front Knee	35	3
Stance Knee	35	3	Back Knee	35	3
Swing Ankle	58	1.32	Back Ankle	58	1.32
Stance Ankle	58	1.32	Back Ankle	58	1.32

Table C2. Control objectives for the global controller: controlled output variable, desired output value (y_{ref}), and weighted output variable (γ); and type of control objective (continuous or end point)

Swing phase				Push off phase			
Controlled variable	y_{ref}	γ	Objective	Controlled variable	y_{ref}	γ	Endpoint
Swing Knee	4	200	endpoint	Speed CoMx	R	100	endpoint
Swing Femur	R	2e3	endpoint	Front Knee	20	100	endpoint
Stance Knee	0	60	continuous				
Trunk	0	200	continuous	Trunk	0	200	continuous

(T) was reconstructed from the desired step length and velocity at push off (Appendix A). The outputs of the system, which are controlled by the GC, are given in Table C2. These outputs are either specified or reconstructed (Appendix A). The global controller regulates these output objectives that are either end-point or continuous conditions.

Acknowledgement. We would like to thank our colleague Dr. Ir. Richard van der Linde, of the Man–Machine Systems and Control Group, Delft University of Technology, for stimulating discussions and suggestions. He has been building an autonomous ballistic bipedal walker.

References

Anderson FC, Ziegler JM, Pandy MG, Whalen RT (1995) Application of high-performance computing to numerical simulation of human movement. J Biomech Eng 117: 155–157

Benbrahim H, Franklin JA (1997) Bipedal dynamic walking using reinforcement learning. Robot Auton Syst 22: 283–302

Chandler RF, Glauser CE, McConville JT, Reynolds HM, Young JW (1975) Investigation of the inertial properties of the human body. Report DOT HS-801430. National Technical Information Service, Springfield, Va.

Garcia CE, Morshedi AM (1986) Quadratic programming solution of dynamic matrix control (QDMC). Chem Eng Comm 46: 73–87

Goswami A, Espiau B, Keramane A (1997) Limit cycles in a passive compass gait biped and passivity-mimicking control laws. J Auton Robot 4: 273–286

Grieve DW, Gear RJ (1966) The relationships between length of stride, step frequency, time of swing and speed of walking for children and adults. Ergonomics 9: 379–399

Hurmuzlu Y (1993) Dynamics of bipedal gait: Part I – Objective functions and the contact event of a planar five-link biped. J Appl Mech 60: 331–336

Inman VT, Ralston HJ, Todd F, Lieberman JC (1981) Human walking. Williams and Wilkins, Baltimore, Md.

Koopman HFJM (1989) The three-dimensional analysis and prediction of human walking. PhD thesis, University Twente, Enschede, The Netherlands

Koopman B, Grootenboer HJ, Jongh HJ (1995) An inverse dynamic model for the analysis reconstruction and prediction of bipedal walking. J Biomech 28: 1369–1376

Kuo AD, Zajac FE (1993) A biomechanical analysis of muscle strength as a limiting factor in standing posture. J Biomech 26 [Suppl 1]: 137–150

Lee JH (1994) Extended Kalman filter based nonlinear model predictive control. Ind Eng Chem Res 33: 1530–1541

Linde RQ van der (1999) Passive bipedal walking with phasic muscle contraction. Biol Cybern 81: 227–237

Lum HK, Zribi M, Soh YC (1999) Planning and control of a biped robot. Int J Eng Sci 37: 1319–1349

Mansour JM, Audu ML (1986) The passive elastic moment at the knee and its influence on human gait. J Biomech 19: 369–373

McGeer T (1990) Passive dynamic walking. Int J Robot Res 9: 62–82

McMahon TA (1984) Mechanics of locomotion. Int J Robot Res 3: 4–28

Mita T, Yamaguchi T, Kashiwase T, Kawase T (1984) Realisation of high speed biped using modern control theory. Int J Control 40: 107–119

Pandy MG, Anderson FC (1999) Three-dimensional computer simulation of jumping and walking using the same model. In: Proceedings of the Seventh International Symposium on Computer Simulation in Biomechanics, University of Calgary, Calgary, Canada, 5–7 August, pp 92–95

Pratt JE, Pratt GA (1999) Exploiting natural dynamics in the control of a 3D bipedal walking simulation. In: Proceedings of the International Conference on Climbing and Walking Robots, Portsmouth, UK, 13–15 September

Raibert MH (1986) Legged robots that balance. MIT Press, Cambridge Mass.

Salatian AW, Yi KY, Zheng YF (1997) Reinforcement learning for a biped robot to climb sloping surfaces. J Robot Syst 14: 283–296

Sardain P, Rostami M, Bessonnet G (1998) An anthropomorphic biped robot: dynamic concepts and technological design. IEEE Trans Syst Man Cybern 28: 823–837

Seo YJ, Yoon YS (1995) Designing of a robust dynamic gait of the biped using the concept of dynamic stability margin. Robotica 13: 461–468

Taga G (1995a) A model of the neuro-musculo-skeletal system for human locomotion. I. Emergence of basic gait. Biol Cybern 73: 97–111

Taga G (1995b) A model of the neuro-musculo-skeletal system for human locomotion. II. Real-time adaptability under various constraints. Biol Cybern 73: 113–121

Van de Belt D (1997) Simulation of walking using optimal control. PhD thesis, Department of Mechanical Engineering, University of Twente, Enschede, The Netherlands

Van Ingen Schenau GJ van (1989) From rotation to translation constraints on multi-joint movements and the unique action of bi-articular muscles. Hum Mov Sci 8: 301–337

Vukobratovic M, Stokic D (1975) Dynamic control of unstable locomotion robots. Math Biosci 24: 129–157

Yamaguchi FT (1990) Performing whole-body simulation of gait with 3-D, dynamic musculo-skeletal model. In: Winters JM, Woo SL-Y (eds) Multiple muscle systems: biomechanics and movement organisation. Springer, Berlin Heidelberg New York, pp 663–679

Yamaguchi GT (1989) Feasibility and conceptual design of functional neuromuscular stimulation systems for the restoration of natural gait to paraplegics based on dynamic muscululoskeletal models. PhD thesis, Department of Mechanical Engineering, Stanford University, Stanford, Calif.

Yang JS (1997) Control of a five link biped using an adaptive inverse dynamic method. Control Comput 25: 56–64

Yoon YS, Mansour JM (1982) The passive elastic moment at the hip. J Biomech 15: 905–910